

# MODELING EFFECTS OF OXYGEN INHIBITION IN MASK BASED STEREOGRAPHY

Amit S. Jariwala<sup>1</sup>, Fei Ding<sup>1</sup>, Aparna Boddapati<sup>2</sup>, Victor Breedveld<sup>2</sup>, Martha Grover<sup>2</sup>, Clifford L. Henderson<sup>2</sup>, David W. Rosen<sup>1\*</sup>

1- George W. Woodruff School of Mechanical Engineering

2- School of Chemical & Biomolecular Engineering

Georgia Institute of Technology

Atlanta, Georgia, 30332

\*Corresponding author. Tel.: +1 404 894 9668 Email: david.rosen@me.gatech.edu

Reviewed, accepted September 23, 2010

## Abstract:

Stereolithography (SL) is an additive manufacturing process in which liquid photopolymer resin is cross-linked and converted to solid with a UV laser light source. Traditional models of SL processes do not consider the complex chemical reactions and species transport occurring during photopolymerization and, hence, are incapable of accurately predicting resin curing behavior. In this paper, a 2D photopolymerization model based on ordinary differential equations is presented that incorporates the effects of oxygen inhibition and diffusion during the polymerization process. This model accurately predicts the cured part height when compared to experiments conducted on a mask based stereolithography system. The simulated results also show the characteristic edge curvature as seen in experiments. Parametric studies were conducted to investigate the possibilities to improve the accuracy of the model for predicting the edge curvature.

## 1. Introduction

Photopolymerization is defined as the reaction of monomers or macromers to produce solid polymeric structures by light-induced initiation and polymerization [1]. Most Stereolithography (SL) resins contain acrylate monomers. For an acrylate resin system, the usual catalyst is a free radical. In Stereolithography, the radical is generated photo chemically. The source of the photo chemically generated radical is a photo initiator, which reacts with an actinic photon. This produces radicals that catalyze the polymerization process. According to Beer Lambert's law of absorption, the exposure ( $\text{mJ}/\text{cm}^2$ ) decreases exponentially with depth [2].

$$E(z) = E_{max} e^{\frac{-z}{D_p}} \quad (1)$$

where  $D_p$  is the resin "penetration depth" (a resin parameter) at the given wavelength and  $E_{max}$  is the exposure at the surface of the resin ( $z = 0$ ). The cured part height,  $z$  is shown in Fig. 1 which shows the schematic of the polymerization process studied in this paper. Based on experimental observations, this model was modified in [3, 4] as follows:

$$z \approx D_{ps} * \ln \left( \frac{D_{pL}}{D_{ps}} * \frac{E}{E_c} + 1 - \frac{D_{pL}}{D_{ps}} \right) \quad (2)$$

The parameters  $E_c$ ,  $D_{pL}$  and  $D_{ps}$  are usually fit to experimental data at a specific resin composition and cure intensity. In practice, polymerization does not proceed beyond a limited depth where the exposure falls below a threshold value,  $E_c$ . This is primarily due to oxygen inhibition, which imposes a minimal threshold to start polymerization. This exposure threshold

model is an oversimplification of the SL process. It directly connects the exposure to the resin and the final solid part shape. It ignores many important intermediate steps. Its ability to predict the three dimensional cured part outline is challenged especially when part resolution is in demand, since it is a one-dimensional model. Therefore, the resin kinetic characteristics, as well as the diffusion effects of oxygen which influence the size, shape and properties of parts fabricated by SL cannot be investigated by using this model. Available chemical models presented in literature only focus on predicting part height and none of them present any approach to predict the shape of the cured profile. We present a unique two dimensional model which can be used to predict part height as well as the shape of the overall cured profile.

The kinetic model for multifunctional acrylate photopolymerization presented here, is based on a set of ordinary differential equations (ODE). The final results show that the kinetic ODE model, based on the critical conversion value, incorporates the impact of process parameters such as initiator concentration, light intensity, oxygen diffusion and exposure time on the final part profile of the object. In addition, the part height predictions from the ODE model are comparable to experiments and the predictions from the modified  $Ec-Dp$  model.

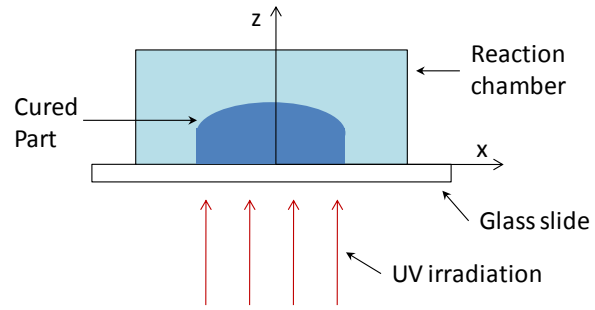


Fig. 1 Schematic of the Polymerization Process

## 2. Polymerization Model

### 2.1 Polymerization Mechanism

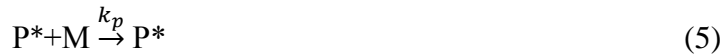
The typical reactants in a photopolymerization reaction are initiator molecules,  $In$ , free radicals generated by initiators,  $R^\bullet$ , polymer chains,  $P$ , monomers,  $M$ , oxygen,  $O_2$ , and solvent, if any. The dynamic concentration of each of these species can be described through a mathematical model based on the reaction mechanism. The reaction mechanism shown in Equations (3)–(12) is used in most photopolymerization simulations [5]. The first step is a decomposition event where an initiator molecule is decomposed to generate two radicals in presence of light.



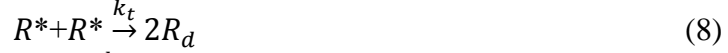
Then, the radical is free to react with a monomer, thus initiating a polymer chain.



Polymer chains propagate via reactions with monomers, or other polymer chains. The polymer grows bigger when reaction occurs between polymer chains. The rate at which this reaction occurs is given by  $k_p$ .



The reactive radical centers on polymer molecules, as well as live radicals, are terminated by reacting either with a free radical or a radical that is on a chain to make dead polymer chains,  $P_d$  and dead radicals,  $R_d$  at a rate of  $k_t$ . Termination can occur either through combination or through disproportionation, and often both mechanisms are present for a given acrylate [6]. In the case of acrylates, it has been found that termination occurs mostly via combination [7].



In addition to the propagation and termination reactions, oxygen in the reaction volume acts as a radical scavenger, and inhibits the propagation and termination reactions. Loss of radicals to oxygen, known as oxygen inhibition, is a problem that is pervasive in polymerization involving radicals [8, 9, 10, 11, and 12]. Oxygen competes strongly for the radicals to form a stable peroxy radical. Until most of the oxygen in the reaction volume has been used up, via reaction with radicals, there is very little consumption of the monomer [8]. The rate at which this reaction proceeds is given by  $k_{toxy}$ .



Equations (3)–(12) contain the typical reactions that take place in photopolymerization systems. These reactions can be simulated through several photopolymerization models. We present the use of ordinary differential equation based models to predict the concentration of reactants in the reaction chamber. The concentration of reactants during the curing process will be used to estimate the thickness and profile of the cured part.

## 2.2 Ordinary Differential Equations

The dynamic concentration of all the species in a well mixed bulk reaction volume can be defined by a set of ordinary differential equations (ODEs) such as the ones shown in Equations (13)–(18) [5].

$$\frac{d[In]}{dt} = -k_d[In] \quad (13)$$

$$\frac{d[R^*]}{dt} = 2k_d[In] - k_p[M][R^*] - 2k_t[P^*][R^*] - 2k_t[R^*]^2 - k_{toxy}[O_2][R^*] \quad (14)$$

$$\frac{d[M]}{dt} = -k_p[M][R^*] - k_p[M][P^*] \quad (15)$$

$$\frac{d[P^*]}{dt} = k_p[M][R^*] - 2k_t[P^*]^2 - 2k_t[P^*][R^*] - k_{toxy}[O_2][P^*] \quad (16)$$

$$\frac{d[P_d]}{dt} = k_t[P^*]^2 + 2k_t[P^*][R^*] + k_{toxy}[O_2][P^*] \quad (17)$$

$$\frac{d[O_2]}{dt} = -k_{toxy}[O_2][R^*] - k_{toxy}[O_2][P^*] \quad (18)$$

The ODE model presented here includes the initiation, propagation, termination and inhibition mechanisms shown in Equations (3)–(12).

In addition to the ODEs presented in Equations (13)–(18), a modification to Equation (18), using the diffusion coefficient  $D_{O_2}$  of the oxygen in monomer, accounts for the oxygen diffusion, as shown in Equation (19).

$$\frac{d[O_2]}{dt} = -k_{toxy}[O_2][R^*] - k_{toxy}[O_2][P^*] - D_{O_2} \left\{ \frac{\partial^2 [O_2]}{\partial z^2} \right\} \quad (19)$$

The solutions to the one dimensional ODEs in Equations (13)–(17) and (19) are used to estimate the concentration of the reactant species. These solutions were validated in [5] for the earlier stages of reaction with a higher intensity light source of wavelength 365nm. Oxygen diffusion only in the vertical direction was included to simulate the mobility of oxygen toward areas that are depleted of oxygen as the reaction progresses. In order to consider the effect of oxygen diffusion in two dimensions, eq. 19 was modified as follows:

$$\frac{d[O_2]}{dt} = -k_{toxy}[O_2][R^*] - k_{toxy}[O_2][P^*] - D_{O_2} \left\{ \frac{\partial^2 [O_2]}{\partial x^2} + \frac{\partial^2 [O_2]}{\partial z^2} \right\} \quad (20)$$

### 3. Material & Rate Constants

#### 3.1 Chemicals used

For the purposes of this study, we used a tri-functional acrylate monomer - Trimethylolpropane Triacrylate (TMPTA, SR-351) obtained from Sartomer. The photoinitiator 2, 2-dimethoxy-1, 2-diphenylethan-1-one (DMPA, IRGACURE-651) was obtained from Ciba Specialty Chemicals. It should be noted that 125 ppm of Hydroxy Quinone (HQ) or 175 ppm of Hydroquinone Monomethyl Ether (MEHQ) are included in the monomer formulation of TMPTA to inhibit polymerization from hydroxy radicals while in storage, and the inhibitor was not removed from the experiments, unless specifically noted. The above ppm concentrations are equivalent to the molar concentration of oxygen in the sample, but the exact amount of inhibitor in the monomer at the time of use can vary, and it has been shown that these inhibitors do not impede the photopolymerization as strongly as Oxygen does [13]. All experiments were neat solutions (containing no additional solvent) of TMPTA prepared at near constant initiator concentration of 5% w/w for TMPTA.

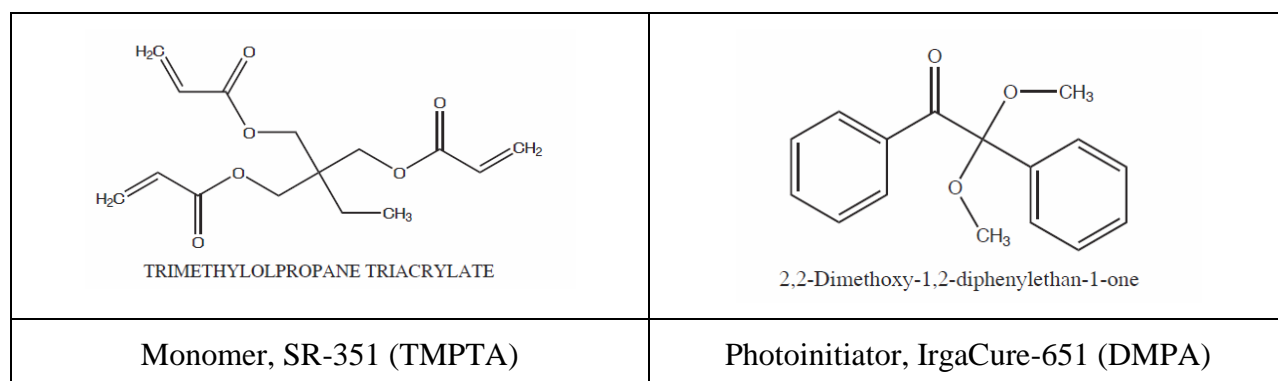


Fig. 2 Structural formula of the monomer and photoinitiator used in this study

### 3.2 Rate Constants and Coefficients

The polymerization reaction starts by the decomposition of initiator molecules into free radicals in the presence of light, as shown in Eq. 3. The rate of initiator decomposition for photopolymerization depends on the concentration of the initiator, the intensity of the light source, and the depth into the absorbing medium [10]. Using the Beer Lambert law, the rate constant for initiator decomposition as a function of depth,  $z$ , into the sample is presented as follows [10, 5]:

$$k_d = 2.3\phi \epsilon [In] I_0 e^{-(2.3\epsilon [In]z)} \left( \frac{\lambda}{N_A h c} \right) \quad (21)$$

Here,  $[In]$  is the concentration of the initiator,  $I_0$  is the incident intensity of the light source. In order to convert the intensity into moles of photons per unit volume, the wavelength of the light in nanometers,  $\lambda$ , Avagadro's number,  $N_A$ , Planck's constant,  $h$ , and speed of light  $c$ , were used.  $\phi$  is the quantum yield of initiation, and it indicates the efficiency of a radical in initiating a polymerization event [10]. In the present case,  $\phi$  was assumed to be 0.6 since that is a typical value for photoinitiators [10].  $\epsilon$  is the molar absorptivity of photons for a given initiator, it depends on the wavelength and temperature, and was determined experimentally by measuring the absorption for known quantities of initiator concentrations in a solvent of known absorption [10, 5].

The rate constants used in subsequent part height predictions, were determined by fitting conversion from the ODE solutions to several experimental data as described in [5]. The following table lists the various rate constants and coefficients used to solve the mathematical model.

**Table 1:** Rate constants and coefficients used to solve ODEs

Parameter	Value	Units	Source
Quantum efficiency of radical, $\phi$	0.6	-	[15]
Molar absorptivity of photons at 325nm wavelength, $\epsilon$	20	m <sup>2</sup> /mol	[15]
UV light Intensity, $I_0$	0.09	W/m <sup>2</sup>	Measured
Molecular weight of Monomer, TMPTA	296	g/mol	Sartomer
Molecular weight of Photoinitiator, DMPA	256	g/mol	Ciba
Rate constant for propagation reaction, $k_p$	0.26	m <sup>3</sup> /mol-s	[5]
Rate constant for termination reaction, $k_t$	0.39	m <sup>3</sup> /mol-s	[5]
Rate constant for termination via oxygen quenching, $k_{toxy}$	2	m <sup>3</sup> /mol-s	[5]
Diffusion coefficient of Oxygen, $D_{O_2}$	1e-10	m <sup>2</sup> /s	[12,16]
Initial concentration of Oxygen, $[O_2]_0$	1.05	mol/m <sup>3</sup>	[17, 11]

### 4. Part Height Estimation

Carothers and Flory described a gel as an infinitely large molecule that is insoluble [18, 19, and 20]. Flory used this definition to estimate the degree of cure necessary for the onset of gelation based on the functionality of the reacting monomers [20]. Once the resin starts to gel,

the viscosity of the solution increases sharply, and the cure undergoes a rapid transition from a liquid state to a solid state [21]. The degree of cure or the monomer conversion is computed using the following formula. The monomer concentration after polymerization is represented as  $[M]$  and the initial monomer concentration is represented as  $[M_0]$ .

$$\text{Conversion} = \frac{[M] - [M_0]}{[M_0]} \quad (22)$$

The shape of the cured part can then be estimated by tracking the coordinates within the sample where the conversion has reached the critical conversion limit. Using the rate constants shown in table 1, a conversion cut-off value of 12% was determined by fitting to the experimental data for TMPTA with oxygen in [5]

## 5. Experimental Setup

The schematic of our Film Micro Stereolithography (FMSL) system is illustrated in Figure 3. The specifications of the system can be found in [4]. The design of the system can be divided into three modules:

**Beam conditioning module:** This module consists of a UV laser light source from Omnicrome (now, Melles Griot) (Model # 3074-M-X04). The laser emits 38.5mW TEM01 at wavelength of 325nm. A beam expander is placed right after the laser source to expand the laser beam diameter from 1.5mm to 15mm. An Engineered™ Diffuser (micro lens array) rotated at rate of 40rpm is used after the beam expander to homogenize the beam's intensity profile and enlarge the beam diameter to 50 mm. A UV transmitting Plano-Convex lens with EFL 150.0 mm is used to collimate the light emerging from the diffuser. A UV coated mirror, mounted on a kinematic mount, directs the laser beam on a dynamic mask.

**Imaging module:** The imaging module consists of a dynamic mask, the Digital Micromirror Device (DMD from Texas Instruments), and an imaging lens (a UV transmitting Plano-Convex lens with an EFL of 100.0 mm). The DMD is an array of individually addressable, bi stable micro mirrors, which can be selectively oriented, to display any bitmap. Every pixel on the bitmap controls one and only one micromirror on the DMD. The micromirrors are 12.65  $\mu\text{m}$  square and the spacing between adjacent micromirrors is 1 $\mu\text{m}$ . The micromirrors in their neutral state are parallel to the DMD chip. In its "ON" state, a micromirror swivels about its diagonal by 12° in one direction and in the "OFF" state, swivels by the same amount in

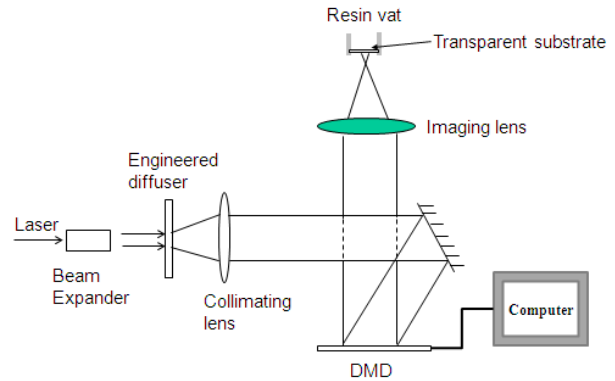


Fig. 3 Schematic of the FMSL system

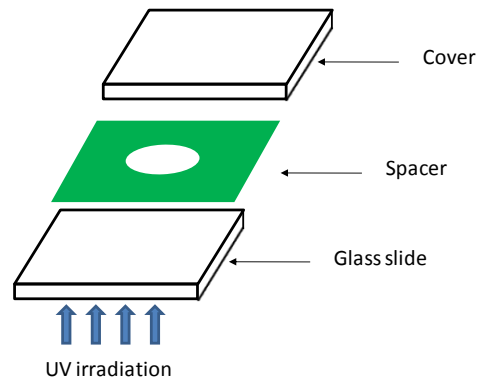


Fig. 4 Schematic of the resin vat

the opposite direction. The bitmap displayed on the DMD is imaged onto the substrate by the imaging lens.

**Resin vat:** The resin vat is composed of a glass substrate, spacer with thickness of 1mm and a plastic cover. The glass substrate is transparent to allow the UV irradiation passing through. The circular hole with diameter of 16 mm in the center of the spacer creates a cylindrical reaction chamber which is sealed by the glass substrate from the bottom and the cover from the top, as shown in Fig. 4.

## 6. Experimental Procedure

The resin in the reaction chamber was cured by the UV irradiation patterned by the bitmaps on DMD. Before experiments, a full bitmap with size of 1024 by 768 is displayed on DMD for 240 seconds to remove oxygen at the top of the glass substrate thus expediting the curing process. Later, a working bitmap with size of 90 by 768 is displayed on DMD to project a rectangular irradiation area at the bottom of the reaction chamber. The full bitmap and the working bitmap are shown in Figure 5. The dark region shows the area where the micromirrors are in “ON” status to project the irradiation into the resin vat. The working bitmap is chosen to be of a rectangular shape so as to match our two dimensional ODE simulations. A surface contact profilometer is used to measure the profile at the central region of the cured part along the width direction.

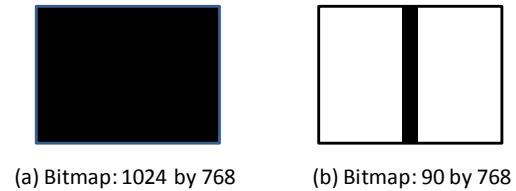


Fig. 5 Bitmaps displayed on DMD

## 7. Numerical FE model

COMSOL simulations were conducted to predict the height and profile of the final cured part. The working bitmap, which has a width of 90 pixels, projects an irradiation region which is 2088  $\mu\text{m}$  wide. A 2D finite element model was created to simulate the experimental conditions. The width of the model was taken as 16mm and the height as 1mm, both of which match the size of the reaction chamber in the actual experimental setup. 2229 triangular elements were used in the simulation. The size of the finest mesh in the irradiation area is 30 $\mu\text{m}$ .

Fig. 6 shows the model of the reaction chamber modeled in COMSOL. The entire rectangular reaction chamber is assumed to be filled with liquid monomer (TMPTA with 5 %w/w of DMPA as photoinitiator). All boundaries are assumed to be insulated, which closely resembles the actual experimental conditions. The coordinate system is also shown in the figure. The

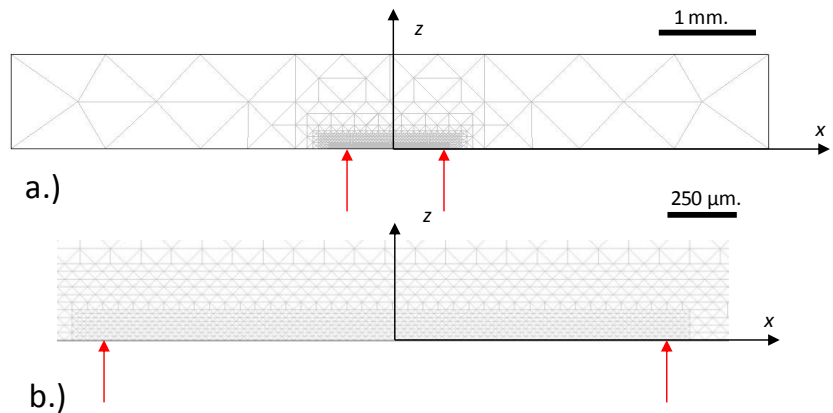


Fig. 6 a.) Schematic of the FE model used in COMSOL; b.) Enlarged view of the FE model

boundary between the red arrows shows the region where irradiation is received by the monomer.

The rate constants from the ordinary differential equations are modeled along with diffusion model (chdi) in COMSOL. The initial concentration of monomer and photoinitiator was calculated as shown in table 2, using the values shown in table 1. Molecular weight for monomer is considered to be thrice the normal weight, as it is a tri-functional monomer

**Table 2:** Calculation for concentration of monomer and photoinitiator

	<b>Monomer Concentration</b>	<b>PI Concentration</b>
Equation	$\frac{3 * (100 - wt \%)}{MW * 0.0001}$	$\frac{wt\%}{MW * 0.0001}$
Molecular Weight, MW	296 g/mol	256 g/mol
Calculated concentration	9628.38 mol/m <sup>3</sup>	195.3125 mol/m <sup>3</sup>

## 8. Results and Discussions

Experiments were performed on our FMSL system. The polymerized parts are cured on the glass slide. The glass slide is removed from the resin vat and additional uncured resin is removed using air duster. A surface contact profilometer (Dektak 3030) was used to measure the cured part profile using the glass slide as the reference. The profile of the cured part showed the maximum part height at the center of the cured region.

Figure 7 shows the comparison of results generated from COMSOL simulations to the modified  $E_c$ - $D_p$  model generated from experimental results. The dashed line in Figure 7 shows the cured height prediction from COMSOL at the center of the cured part. The exposure is calculated as the product of irradiated intensity and curing time (including the time for which the full bitmap was switched on). For cured height less than 80 $\mu$ m, COMSOL simulation results match very well with experiments. This observation is consistent with [5], since the rate constants used in our simulations were optimized for lower curing time.

The modified  $E_c$ - $D_p$  empirical model can only predict the cured height and it has no means to capture the cured shape which is

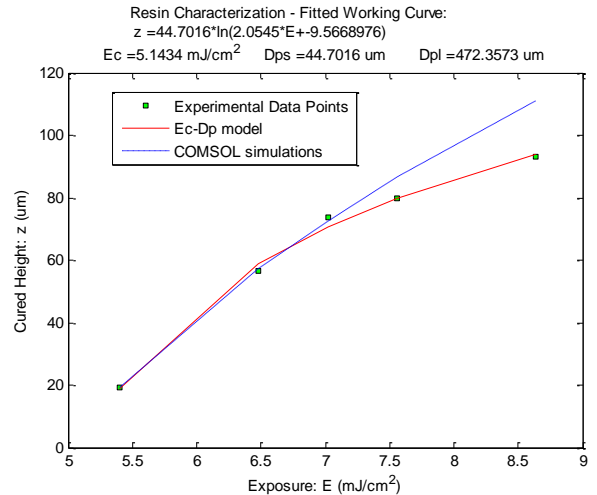


Fig. 7 Comparison between the predicted height from COMSOL and experiments

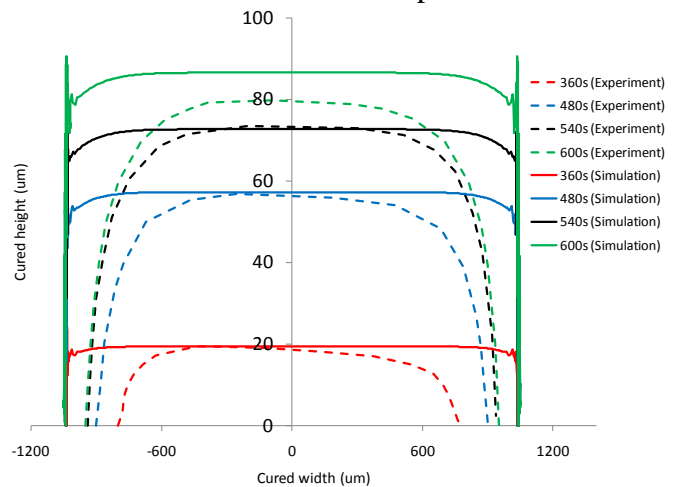


Fig. 8 Comparison between the predicted profile of cured part from COMSOL and experiments

generated by stereolithography process. Since, we modeled the polymerization process with oxygen diffusion in two dimensions, COMSOL simulation results can be used to simulate the cured shape. Figure 8 shows the cured profile generated from experiments for various curing times. The solid lines show the predicted profile of the cured part for different energy doses provided.

The profiles from simulation do not match with the experiments towards the edge of the sample, although the simulation shows a curvature on the

edge of the cured part. Another observation from Figure 8 is that the width of the actual cured part is always lesser than the width of the irradiation area. However, none of the COMSOL predictions show this width reduction. We observe that the cured width increases with an increase in curing time (and hence the total energy dose). A potential explanation for the mismatch in edge profile and width reduction maybe that the rate constants and other coefficients are assumed to be independent of time and location in the reaction chamber in our study. This assumption needs further in depth studies before this model can be used for predicting edge profiles.

We studied the effect of variation of diffusivity and concentration of oxygen on the predicted profile of cured part in COMSOL for a total curing time of 540s. Figure 9 shows that varying the coefficient of oxygen diffusion coefficient do not help predict the severe curvature as observed at the edge of the cured part.

Figure 10 shows the effects of varying oxygen concentration for curing

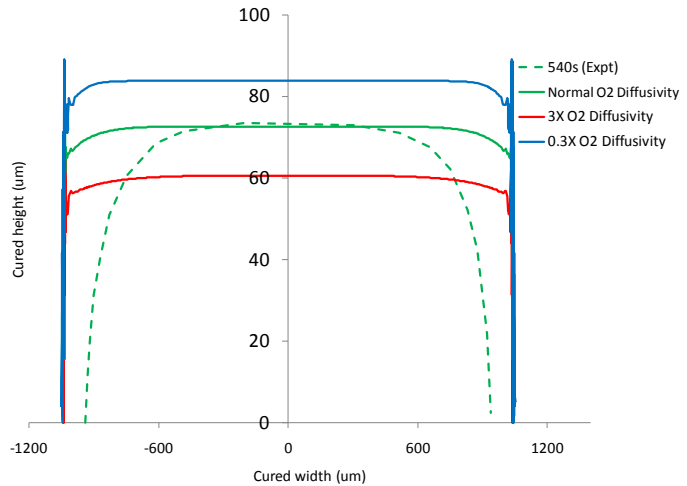


Fig. 9 Plot showing effect of varying oxygen diffusivity on predicted part profile in COMSOL

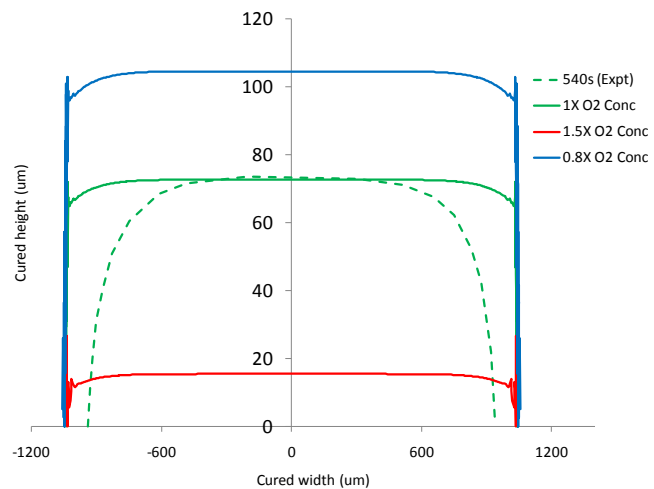


Fig. 10 Comparison between the predicted profile of cured part from COMSOL and experiments

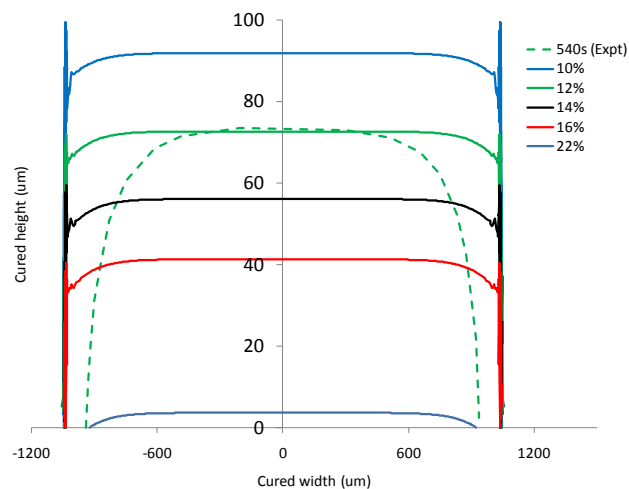


Fig. 11 Effect of varying monomer conversion %

time of 540s. Increasing or decreasing the initial concentration of oxygen has very little effect on the shape of the edge profile. However, this change has significant effect on the predicted height of the cured part.

Figure 11 shows the plot of different monomer conversion cut-off percentages. Varying monomer conversion cut-off values do not help to estimate the reduced width as seen in experimental observations, except when using a very high cut-off value, which cannot be used to predict the height.

The width reduction in the cured parts maybe attributed to shrinkage. From an industry report for SR-351 [22], shrinkage of 28% percent was observed when the part was fully cured (i.e., 100% monomer conversion). During the curing process, shrinkage would occur dynamically as the resin receives larger energy dose and starts to grow in the height direction. We did not find any studies which report the shrinkage of SR-351 during the curing process (i.e., when the monomer has not fully cured and the conversion percent is lesser than 100%). This dynamic shrinkage process has to be further understood in order to improve our polymerization model.

## 9. Conclusions

This paper presented a unique approach to predict the shape of a part cured by photopolymerization. We used two dimensional ordinary differential equations to simulate the photopolymerization process in order to predict the cured part profile for curing a tri-functional acrylate monomer. These equations incorporated the chemical kinetics and oxygen diffusion and were solved by using COMSOL. The simulated results matched the experimental observation for predicting the part height.

The presented model could be further improved to explain the reduction of part width and the curvature observed at the edges of the cured part. These improvements can be made by optimizing the chemical rate constants and incorporating the effects of shrinkage in our photopolymerization model.

## 10. References

- [1] Decker, C. , “Photoinitiated Curing of Multifunctional Monomers”, *Acta Polymer*, 43, pp. 333-347, 1994.
- [2] Jacobs, P., “*Rapid Prototyping & Manufacturing: Fundamentals of Stereolithography*”, Dearborn, MI., *Society of Manufacturing Engineers*, 1992.
- [3] Limaye, A., & Rosen, D., “Process Planning Method for Mask Projection Micro-Stereolithography”, *Rapid Prototyping Journal* , 13 (2), pp. 76-84, 2007.
- [4] Jariwala, A., Ding, F., Zhao, X., & Rosen, D. W., “A Process Planning Method for Thin Film Mask Projection Micro-Stereolithography”, *Proceedings of the ASME 2009 International Design Engineering Technical Conferences & Computers and Information in Engineering Conference*. San Diego, CA, Paper no. DETC2009-87532, 2009.
- [5] Boddapati, A., “Modeling Cure Depth during Photopolymerization of Multifunctional Acrylates”, M.S. Thesis, Georgia Institute of Technology, School of Chemical & Biomolecular Engineering, Atlanta, 2010.

- [6] Bowman, C. N. and Peppas, N. A., "A kinetic gelation method for the simulation of free-radical polymerizations," *Chemical Engineering Science*, 47(6), pp. 1411–1419, 1992.
- [7] Moad, G. and Solomon, D., "*The Chemistry of Radical Polymerization*", pp. 233–278, Oxford: Elsevier, 2<sup>nd</sup> ed., 2006.
- [8] Decker, C. and Jenkins, A. D., "Kinetic approach of oxygen inhibition in ultraviolet-induced and laser-induced polymerizations," *Macromolecules*, 18(6), pp. 1241–1244, 1985.
- [9] Lovestead, T. M., O'Brien, A. K., and Bowman, C. N., "Models of multivinyl free radical photopolymerization kinetics," *Journal of Photochemistry and Photobiology a-Chemistry*, 159(2), pp. 135–143, 2003.
- [10] Odian, G., "Radical chain polymerization", *Principles of Polymerization*, pp. 198–349, New York: John Wiley & Sons, 4<sup>th</sup> ed., 2004.
- [11] Gou, L. J., Coretsopoulos, C. N., and Scranton, A. B., "Measurement of the dissolved oxygen concentration in acrylate monomers with a novel photochemical method," *Journal of Polymer Science Part A – Polymer Chemistry*, 42(5), pp. 1285–1292, 2004.
- [12] O'Brien, A. K. and Bowman, C. N., "Impact of oxygen on photopolymerization kinetics and polymer structure," *Macromolecules*, 39(7), pp. 2501–2506, 2006.
- [13] Slopek, R., "In-Situ Monitoring of the Mechanical Properties during the Photopolymerization of Acrylate Resins Using Particle Tracking Microrheology", PhD thesis, Georgia Institute of Technology, Atlanta, 2008.
- [14] Goodner, M. and Bowman, C., "Modeling and experimental investigation of light intensity and initiator effects on solvent-free photopolymerization," *National Meeting of the American Chemical Society*, Las Vegas, Nevada (Long, T. and Hunt, M., eds.), 713, pp. 220–231, American Chemical Society, 1998.
- [15] Tang, Y., "*Stereolithography Cure Process Modeling*", PhD thesis, Georgia Institute of Technology, Atlanta, 2005.
- [16] O'Brien, A.K. and C.N. Bowman, "Modeling the effect of oxygen on photopolymerization kinetics", *Macromolecular Theory and Simulations*, 15(2), pp. 176-182, 2006.
- [17] Nunes, T.G., L. Ceballos, R. Osorio, and M. Toledano, "Spatially resolved photopolymerization kinetics and oxygen inhibition in dental adhesives." *Biomaterials*, 26(14), pp. 1809-1817, 2005.
- [18] Carothers, W. H., "Polymerization," *Chemical Reviews*, vol. 8, no. 3, pp. 353–426, 1931.
- [19] Carothers, W. H., "Polymers and polyfunctionality," *Transactions of the Faraday Society*, 32(1), pp. 0039–0053, 1936.
- [20] Flory, P. J., "Molecular size distribution in three dimensional polymers. I. gelation," *Journal of the American Chemical Society*, vol. 63, pp. 3083–3090, 1941.
- [21] Winter, H. H. and Chambon, F., "Analysis of linear viscoelasticity of a crosslinking polymer at the gel point," *Journal of Rheology*, 30(2), pp. 367–382, 1986.
- [22] <http://www.sartomer.com/TechLit/4029.pdf>; visited on 6/15/10.